中國機械工程學刊第四十三卷第六期第 559~567 頁(民國一百一十一年)
Journal of the Chinese Society of Mechanical Engineers, Vol.43, No.6, pp.559~567(2022)

# Experimental Investigation of Friction Stir Weldability of AA 7075 Alloy

Sertan Ozan*, Safa Şahin** and Şefika Kasman***

**Keywords** ： aluminum alloy, friction stir welding, macrostructure, microstructure, mechanical properties.

## ABSTRACT

This study focused on process factors, namely welding speed and tool rotation speed, to investigate the friction stir welded joint characteristics of AA 7075-T651 aluminum alloy via microstructural and mechanical properties. On the weld created using the parameters of 40 mm/min welding speed and 630 rpm tool rotation speed, the coarsest grain size measured was 3.75 μm; however, the finest grain with a size of 2.37 μm was measured on the welded joint produced with 80 mm/min welding speed and 800 rpm tool rotation speed. The tensile strength with the highest value was achieved when welding parameters were set at 800 rpm tool rotation speed and 80 mm/min welding speed. The defective joints exhibited lower tensile strength and ductility. Hardness measurement results revealed that each welded joint had a "W" hardness profile.

## INTRODUCTION

Welding, one of the secondary processes in the industry, has a wide application area. It has primary importance in joining parts with different geometries, especially in the aviation, automotive, and ship industries. Welding processes may be classified into two types based on the energy utilized to join metals: solid-state and fusion welding methods. There is a need for local melting of plates to be welded in all fusion welding applications. In applications where melting is involved, protecting the fusion zone from the reactive effect of air is a critical issue.

*Paper Received March, 2022. Revised October, 2022. Accepted November, 2022. Author for Correspondence: Sertan Ozan.*

* *Associate Professor, Department of Mechanical Engineering, Yozgat Bozok University, Yozgat 66100, Turkey*

** *Graduate Student, Department of Mechanical Engineering, Yozgat Bozok University, Yozgat 66100, Turkey*

*** *Associate Professor, Department of Mechanical Engineering, Dokuz Eylul University, Izmir 35397, Turkey*

In cases where the required protection is not provided, the presence of defects that cause the strength of the weld bond to be lower could be possible. Notably, controlling the melting zone's solidification rate affects the weld bond's strength. In this respect, considering the chemical content of some metals, it is challenging to reduce and eliminate the effects of weld defects on the weld bond's strength in fusion welding processes. Production of defect-free welded joints is possible using solid-state welding applications for some metals. In solid-state welding, welding defects caused by the nature of fusion welding processes are not detected, making the solid-state welding process the most important and effective alternative to fusion welds (Kasman & Ozan, 2019, 2020a, 2020b; Ozan, 2020; Ozan, Sahin, & Kasman, 2022).

The poor weldability of particular aluminum alloys through fusion welds can be attributable to specific characteristics, such as limited cooling rate control and a rigid oxide layer (Lakshminarayanan, Balasubramanian, & Elangovan, 2009). Taking aluminum alloys into consideration, it could be challenging to control the solidification of heat-treatable alloys, i.e., phase transformations in welding applications at high temperatures worsen the welded joints' mechanical and microstructural properties. The AA 7XXX series alloys are often regarded as the most "difficult-to-weld" when employing fusion welding procedures. AA 7075 aluminum alloy, one of the AA 7XXX series alloys, is in the Al-Zn-Mg-Cu group (Xu, Li, & Sun, 2017). AA 7075 aluminum alloy is used in various industries due to its remarkable features, which include a high strength-to-density ratio and excellent fatigue strength (Xu et al., 2017). The weldability of AA 7075 aluminum alloys is relatively poor when fusion welding techniques are preferred (Xu et al., 2017). Aluminum alloys find broad application areas due to their lightweight, high strength-to-weight ratio, and ease of design features (Kah, Rajan, Martikainen, & Suoranta, 2015).

Friction stir welding (FSW) is one of the most preferred methods of joining aluminum, magnesium, and copper alloys (Seidel & Reynolds, 2001). The FSW method allows metals to be joined without requiring any filler material (Seidel & Reynolds,

2001). FSW is a solid-state welding procedure during which the joined metals do not melt; notably, no defects originate from the melting process (Lakshminarayanan et al., 2009). Many studies have been carried out, and successful results have been achieved in the joining process of aluminum alloys with FSW, continuing to develop today. Those studies (Kasman & Ozan, 2019, 2020a, 2020b; Ozan, 2020; Ozan, Sahin, & Kasman, 2022) revealed that the FSW method could give positive results in the joining process of aluminum alloys. For the aluminum alloys regarded as "difficult to weld" utilizing fusion welding techniques, the FSW has started to be preferred in many industrial welding applications, especially in the fields of aircraft, automotive, and shipbuilding industries (Ma, Feng, Chen, & Shen, 2018; Sharma, Dwivedi, & Kumar, 2012).

The way the FSW method is applied differs from the fusion welding methods. The workpieces are positioned face to face on a specially prepared workbench table in this method. Following this placement, the plates should be rigidly fixed. Their positions do not change with the rotation effect of the stirring tool. The friction between the tool components and the plates generates the heat necessary for the FSW process. Shoulder and pin are the names of the two components that form the tools used in the welding procedures. In most applications, those two parts are monolithic. Before the welding process, the pin of the rotating tool is immersed in the surface where the weld metals are in contact, and when the shoulder contacts the upper surface of the metals, the tool is rotated without moving for a while (Sadoun, Meselhy, & Deabs, 2020). The aim is to ensure that sufficient frictional heat is obtained for the welding process. The heat provided by the friction effect causes the metals to soften and become ductile along a certain width from the contact surfaces (Sadoun et al., 2020). FSW is a welding method in which both extrusion and forging processes work together, and FSW takes place with the effect of plastic deformation (Kumar et al., 2011; Rajak et al., 2020; Rezaei, Mirbeik, & Bisadi, 2011; Zhang et al., 2012). FSW consists of five distinct steps, namely preheating, initial deformation, extrusion, forging, and post-weld cooling down, as reported elsewhere (Backar, Elhofy, & Nassef, 2020). The local softening of the metals by the heat generated from the friction between the tool and the plates facilitates the movement of the tool along the contact line. Notably, the deformation ability of weld metals increases depending on the severity of friction heat. With the effect of rotation, advancement, and mixing, the tool carries the materials to the space it leaves behind. The metal on the front edge of the tool is carried by the tool-pin, which takes the metal on the other side of the tool-pin and transfers it to the gap on the other side of the welding process direction. Thus, a weld bond is established between the two metals with this repeated process along the welding line (Thomas, 1998). The weld bond is formed by the forging and extrusion effect of the tool-shoulder (Kumar, Kailas, & Srivatsan, 2011; Rajak, Pagar, Menezes, & Eyvazian, 2020; Zhang, Cao, Larose, & Wanjara, 2012).

The softened metal formed by the rotating tool creates the first deformation zone. With the deformation occurring in this region, the metal is first forced to move upwards and then downwards by the forging effect of the shoulder part, creating a kind of extrusion process. It provides the formation of the extrusion zone with this successive metal movement. When the tool is moved in the forward direction, in the extrusion zone, the tool pin moves the metal forward, transferring it to the gap created by the pin with its rotational movement. The tool shoulder forges the extruded metal and provides a consolidated structure on the processed area. After the weld bond is formed, the metal cools in the process area (Rajakumar, Muralidharan, & Balasubramanian, 2011; Rezaei et al., 2011). The weld bond consists of two characteristic edges, defined according to the position of the metal to be welded and the rotation direction of the tool. Assume the metal is in the tool's rotational direction; in such case, it is referred to as the advancing side (AS). If it is in the opposite direction of the tool's rotation or the opposite direction of the tool's advancement, it is regarded as the retreating side (RS). However, both sides consist of four distinct regions, namely base metal (BM), heat affected zone (HAZ), thermo-mechanically affected zone (TMAZ), and stir zone (SZ) (Thomas, Johnson, & Wiesner, 2003). Different types of defects could occur in FSW methods peculiar to its solid-state joining process (Kasman & Ozan, 2019, 2020a, 2020b; Ozan, 2020; Ozan, Sahin, & Kasman, 2022).

The literature survey related to the FSW of AA 7075 revealed that the FSW parameters of tool rotation speed (TRS), welding speed (WS), and pin profile were influential on the mechanical and microstructural attributes of joints (Dehghani, Ghorbani, & Soltanipoor, 2015; Farzadi, 2017; Mao, Ke, Chen, Liu, & Xing, 2017; Patel, Badheka, & Kumar, 2017; Rajakumar et al., 2011; Xu et al., 2017). A straightforward approach has not yet been achieved in determining friction stir welding parameters of AA 7075 aluminum alloy. The tool design and selected welding settings distinguish this study from the existing literature. The tool, with its design, provided successful results. The present study concentrated on the FSW parameters to determine the welded joint characteristics using UTS and $\varepsilon_R$ (%), aiming to determine better FSW parameter combinations using a helical profiled pin.

## EXPERIMENTAL STUDIES

The material of the plates used in FSW applications was AA 7075-T651 aluminum alloy. Table 1 presents the mechanical characteristics of AA 7075-T651. According to the preliminary studies and research on FSW (Kasman & Ozan, 2019; Ozan, Sahin, & Kasman, 2022), the parameters coordinating the FSW for building a weld bond between two plates are TRS, WS, tool-shoulder diameter, tool-pin geometry, tool rotation direction, inclined angle, and tool-pin penetration. The tool rotation direction, the inclined angle, and the amount of tool pin penetration were selected clockwise, two degrees and 4.95 mm, respectively; and WS and TRS values were selected in accordance with our previous study (Ozan, Sahin, & Kasman, 2022). During the FSW experiments, a tool with a 20 mm shoulder diameter and a helically threaded pin with a 1 mm pitch was used. The tools were manufactured from AISI H13 hot work tool steel, and their hardness was adjusted to 50-52 HRC via heat treatment. The FSW components and tool pin geometry used in the experimental studies are shown in Figs. 1a and 1b. The surfaces of the plates used in welding applications were processed to remove the burrs from the cutting process, thus providing dimensional tolerances and removing the oxide layer and residues on the surface. It is well-known that a relevant surface cleaning process is crucial, ensuring complete contact with the joining surfaces. As shown in Fig. 1a, the plates to be joined were fixed to a backing plate.

Table 1. Mechanical properties of the alloy AA 7075-T651.

| *Ultimate Tensile Strength (MPa) | *Elongation at rapture (%) | Hardness (HV) |
|---|---|---|
| 535±5 | 12±1 | 182±2 |
| * Ref. (Ozan, Sahin, & Kasman, 2022) | | |

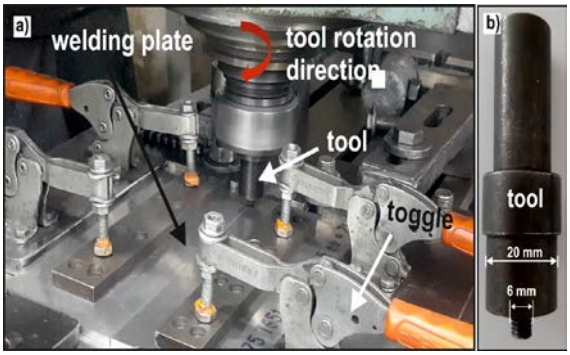

Fig. 1. (a) Friction stir welding components; (b) Tool.

The steps of the FSW application are seen in Fig. 2. Considering the preliminary studies (Kasman & Ozan, 2019; Ozan, Sahin, & Kasman, 2022), the tool pin's dwell contact time between the welded plates was determined to be 20 s. For the macrostructure and microstructure analyses, standard metallography procedures were applied to the cross-sectioned surface of the welded joint. Following the surface polishing process for optical microscope examinations, the specimens were etched in Keller solution and kept for 105 s for macroscopic examinations and 45 s for microscopic examinations.

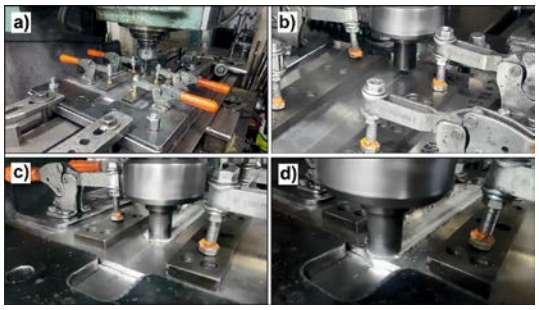

Fig. 2. Stages of friction stir welding process (a) Tool-pin's approach to the plates; (b) Plunging of the tool-pin between the plates; (c) Advance movement of the tool-pin; (d) Completion of the weld seam.

The laser cutting machine was used to cut tensile test specimens with a gauge section of 50 mm by 12.5 mm by 5 mm. Tensile testing was conducted with a cross-head speed of 2 mm/min using a device of the Shimadzu brand and model AGS-X. The device had a load capacity of 100 kN. Following the tensile test, the elongation at the rapture ($\varepsilon_R$) and ultimate tensile strength (UTS) was measured to evaluate the tensile characteristics of the welded joints. The Quanta brand FEG 450 model scanning electron microscope (SEM) was used to make the microstructural observations on the cross-sectional surfaces of the welded joints. The cross-sectional surfaces of the welded joints were evaluated for their microhardness to create a hardness profile that began at the base metal of the AS and continued all the way to the base metal of the RS. The Metkon MH-3 brand of hardness equipment was used to measure surface hardness, and a load of 100 g was applied for 15 seconds at intervals of 1 mm.

## RESULTS AND DISCUSSION

The macrostructures of the welded joints produced using a tool with the helical geometry pin are shown in Fig. 3. Macrostructural observation of the cross-section of the welded joints revealed that the SZ exhibited a basin-like form. The TRS and WS did not lead to a significant difference in the shape of the SZ (Fig. 3). Tool pin geometry was reported to be influential on the shape of the SZ (Patel et al., 2017).

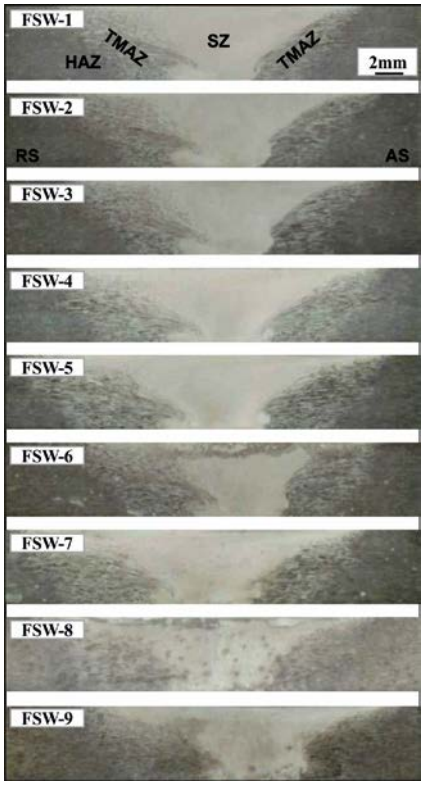


Fig. 3. Macrostructure of the friction stir welded joints.

Defective welded joints were observed to contain cavity-type defects and voids on the AS of the weld root (Fig. 4). Cavity-type defects on the AS of the weld root were similar in size and shape. The improper material movement due to turbulence originating from the pulsation action results in the formation of cavities in the welded joint. (Patel et al., 2017). Additionally, insufficient heat also causes the formation of cavity-like defects to occur. The presence of voids in the weld seam is attributed to insufficient material transfer, improper flow motion, and stirring action (Albannai, 2020). The improperly selected welding parameters, TRS, WS, and pin profile, are responsible for the defects in a welded joint (Albannai, 2020). It is well-known that any defect results in a reduction in weld strength and ductility. FSW 1, 2, 5, and 6 welded joints seen in Fig. 4 had cavity-type defects. It was revealed that welded joints exhibited onion rings, as seen in Fig. 5. Onion rings are a geometrical phenomenon with a ring shape created by plastic deformation during FS welding. The shapes in the onion rings are formed by the layered agglomeration of the extruded material; the stirred materials pile up at each turn with the effect of plastic deformation, as reported elsewhere (Mao et al., 2015). A weld seam produced using FSW is shaped by the effects of a continuous forging and extrusion process; however, the welding parameters and the heat input controlled by the tool have the most significant influence on the quality of the welded joint.

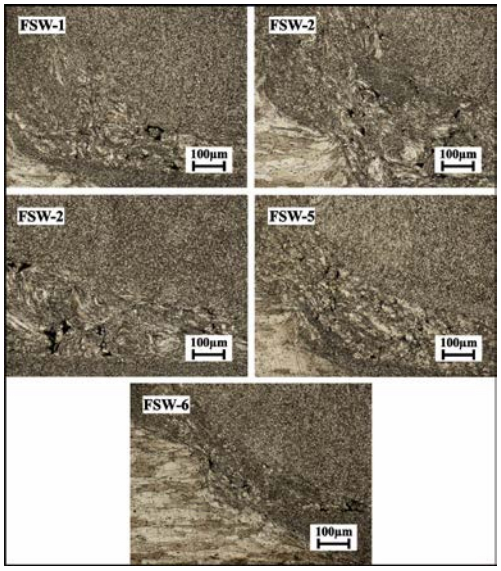


Fig. 4. Optical micrographs of defective friction stir welded joints.

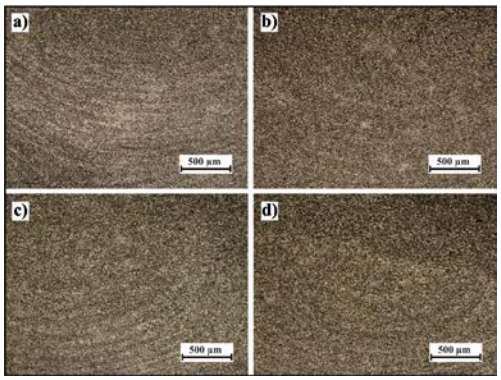


Fig. 5. Optical micrographs belonging to onion ring formation of friction stir welded joints (a) FSW-1; (b) FSW-2; (c) FSW-5; (d) FSW-6.

The presence of defects is highly affected by the plastic flow and heat. Additionally, the intensity of heat generation and plastic flow dominates SZ's dynamically recrystallized grain sizes. The grain size measurements were performed on SZ grains for each welded joint. Fig. 6 exhibits the SZs' microstructure used in grain size measurements. While keeping the TRS constant, the grain size decreased with the increase in WS, as seen in Fig. 7a and Table 2. The grain sizes were detected to be varied between 3.75 and 2.37 μm. While the coarser grain size with a value of 3.75 μm was measured with the FSW process of 630 rpm TRS and 40 mm/min WS, the finer grain size with a value of 2.37 μm was measured with the FSW process of 800 rpm TRS and 80 mm/min WS. Taking the highest welding speed into account, lower heat input resulted in finer grain size. The lowest grain size measured at 630 rpm TRS was 2.48 μm; it is worth noting that an increase in WS from 40 mm/min to 80 mm/min led to a dramatic decrease in grain size. An increase in WS causes a decrease in heat input per unit area (Gemme,

Verreman, Dubourg, & Wanjara, 2011; Mao et al., 2015). The highest grain size measured at 800 rpm TRS was 3.23 µm. The grain size change in welding speed from 40 mm/min to 80 mm/min at 800 rpm was lower than at 630 rpm. An increase in WS when the TRS was set at 400 rpm led to a decrease in grain size.

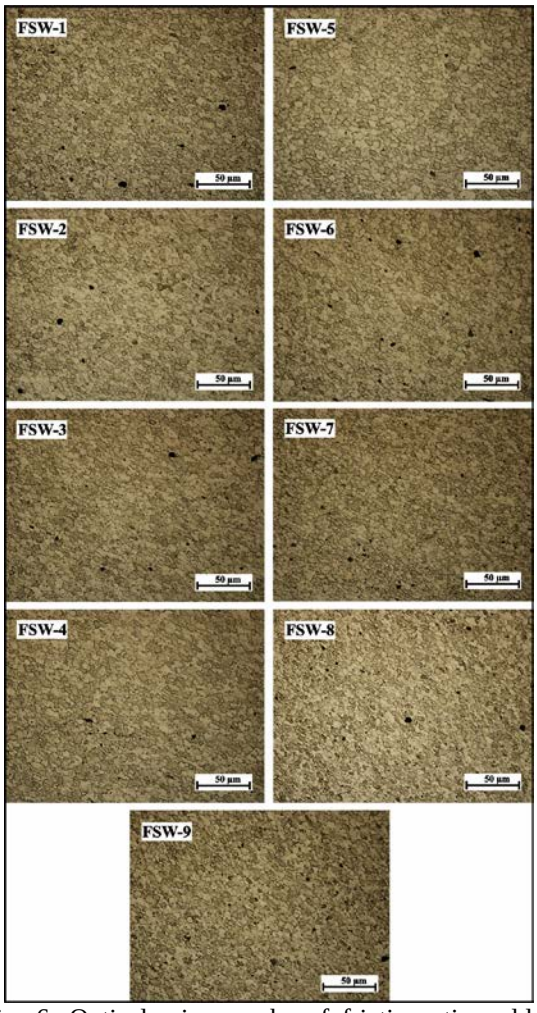


Fig. 6. Optical micrographs of friction stir welded joints corresponding to the stir zone.

Table 2. Tensile characteristics of the joints.

| Joint No | TRS | WS | UTS | $\varepsilon_R$ | WE for UTS | WE for $\varepsilon_R$ | Average grain size |
|---|---|---|---|---|---|---|---|
| FSW-1 | 400 | 40 | 293±5 | 2±0 | 55 | 17 | 2.73±0.24 |
| FSW-2 | 400 | 63 | 234±21 | 1±0 | 44 | 8 | 2.69±0.28 |
| FSW-3 | 400 | 80 | 316±12 | 3±1 | 59 | 25 | 2.53±0.16 |
| FSW-4 | 630 | 40 | 333±2 | 6±1 | 62 | 50 | 3.75±0.53 |
| FSW-5 | 630 | 63 | 279±13 | 1±0 | 52 | 8 | 3.30±0.29 |
| FSW-6 | 630 | 80 | 297±28 | 2±1 | 56 | 17 | 2.48±0.21 |
| FSW-7 | 800 | 40 | 315±5 | 4±0 | 59 | 33 | 3.23±0.24 |
| FSW-8 | 800 | 63 | 343±10 | 4±1 | 64 | 33 | 2.74±0.21 |
| FSW-9 | 800 | 80 | 346±14 | 4±1 | 65 | 33 | 2.37±0.35 |

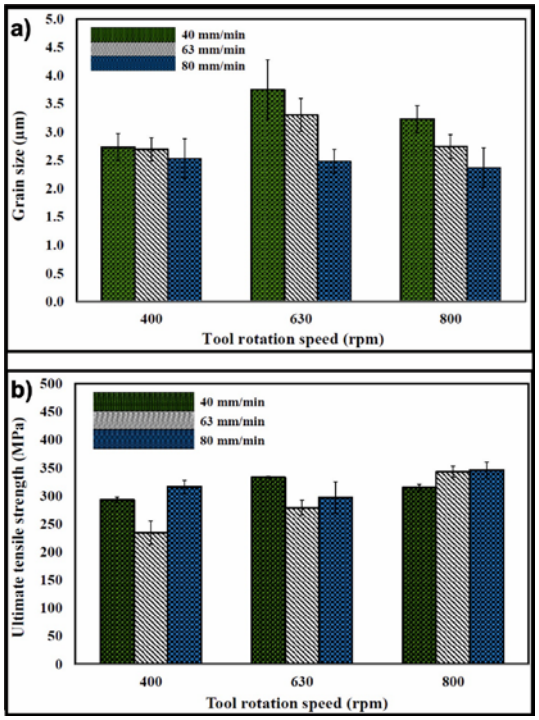


Fig. 7. (a) Grain size values of joints;
(b) Ultimate tensile strength of joints.

AA 7075-T651 aluminum alloy is a precipitation-hardened alloy with $MgZn_2$ second phase particles (Mao et al., 2017; Rajakumar et al., 2011; Sharma, Dwivedi, & Kumar, 2014). It was revealed that secondary particles and strengthening precipitate with different sizes and shapes occurred in the SZ (Fig. 8), as reported elsewhere (Mahoney, Rhodes, Flintoff, Spurling, & Bingel, 1998; Shah & Badheka, 2016). The EDS analysis results belonging to FSW-9 welded joint, seen in Fig. 9, revealed that the particle seen in Spot 1 was rich in Zn (5.81%), Mg (2.74%), Fe (2,25%), Cu (2%). The relevant particle could be identified as the Fe-rich and Mg-Cu-Zn particles, as reported elsewhere (Utyaganova et al., 2021). The particle, seen in Spot 2, Spot 3, and Spot 4, was rich in Zn, Mg, and Cu, as given in Fig. 9. The particle could be Mg(Zn, Cu, $Al)_2$ phase and ($Al_2Mg_3$(Cu, $Zn)_3$) as reported elsewhere (Hua, Hu, & Han, 2020; Zou, Yan, & Chen, 2017).

The effects of FSW parameters on the tensile properties were investigated, and results were reported in Table 2 and Fig. 7b. The variation in UTS values for 400 rpm and 630 rpm TRS depending on WS exhibited a similar trend. While the UTS decreased between 40 mm/min and 63 mm/min WS, it increased between 63 mm/min and 80 mm/min WS. However, any increase in WS for 800 rpm led to an increase in UTS. The $\varepsilon_R$ of defective welds was lower, meaning that they fractured in a brittle manner. The highest $\varepsilon_R$ was measured to be 6%; the relevant welded joint was produced with the FSW condition of 630 rpm TRS and 40 mm/min WS. This $\varepsilon_R$ value

is half the $\varepsilon_R$ value of the base metal. The UTS value at this condition was measured to be 333 MPa. The weld efficiency belonging to UTS and $\varepsilon_R$ for each welded joint was calculated, and the results are listed in Table 2.

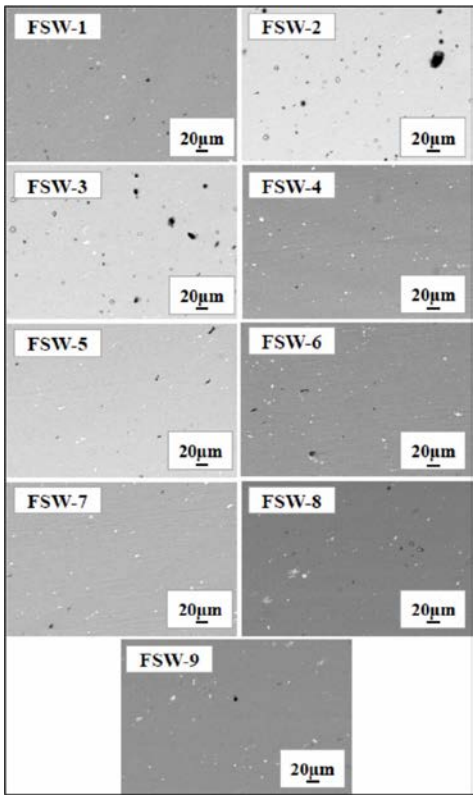


Fig. 8. The dispersion of secondary phase particles in joints.

The values of the mechanical characteristics reported in Table 2 were determined using the results of three different tensile tests. These tests were carried out to ensure the results' accuracy. One can calculate the weld efficiency (WE,%) for UTS by dividing the UTS value of the experimental welding condition by the UTS value of the base metal. The formula ($UTS_{FSW}/UTS_{BM}$) is multiplied by 100, representing the weld efficiency for UTS. On the other hand, weld efficiency (WE,%) for elongation at rapture [($\varepsilon_{R\text{-}FSW}/\varepsilon_{R\text{-}BM}$) × 100] may be computed by dividing the elongation at rapture value of the experimental welding condition by the elongation at rapture value of the base metal, resulting in a percentage that represents the weld's efficiency. The highest UTS efficiency was calculated to be 65% for FSW-9; FSW-4 exhibited the highest $\varepsilon_R$ efficiency with a value of 50%. The fracture location of each welded joint is given in Fig. 10. FSW-1, 2, 3, 5, and 6 were fractured in SZ; however, FSW 7-8 were fractured outside the SZ between HAZ and the base metal of AS. The fracture site of FSW-4 was between HAZ and the base metal of RS. Notably, it is impossible to exhibit how much the stir zone grain size affected the tensile strength of the welded joints. Because of the defects in the welded joints, some of them fractured in the SZ. It would be incorrect to associate SZ grain size with tensile strength in this case. To be compared, all welded joint specimens are required to be free of flaws.

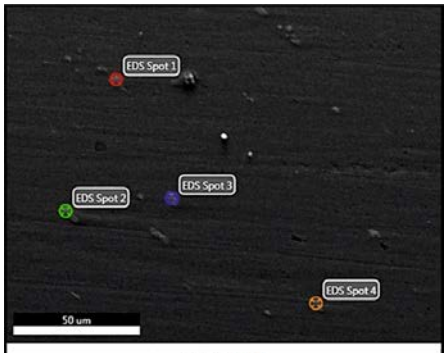


| EDS Spot 1 | | |
|---|---|---|
| Element | Weight (%) | Atomic (%) |
| CuL | 2.01 | 0.9 |
| ZnL | 5.81 | 2.53 |
| MgK | 2.74 | 3.22 |
| AlK | 87.19 | 92.2 |
| FeK | 2.25 | 1.15 |

| EDS Spot 2 | | |
|---|---|---|
| Element | Weight (%) | Atomic (%) |
| CuL | 1.15 | 0.51 |
| ZnL | 5.61 | 2.4 |
| MgK | 2.72 | 3.14 |
| AlK | 90.52 | 93.95 |

| EDS Spot 3 | | |
|---|---|---|
| Element | Weight (%) | Atomic (%) |
| CuL | 0.98 | 0.43 |
| ZnL | 5.62 | 2.41 |
| MgK | 2.66 | 3.06 |
| AlK | 90.73 | 94.1 |

| EDS Spot 4 | | |
|---|---|---|
| Element | Weight (%) | Atomic (%) |
| CuL | 0.76 | 0.34 |
| ZnL | 6.01 | 2.58 |
| MgK | 2.89 | 3.32 |
| AlK | 90.34 | 93.76 |

Fig. 9. The EDS analysis results of FSW-9 welded joint.

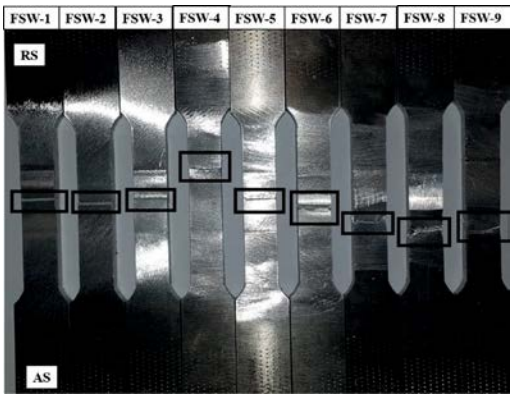


Fig. 10. Fracture location of joints.

The welded joints' hardness profile with the changing WS is shown in Fig. 11. According to the findings of hardness measurements taken at 1 mm

intervals from the base metal, the hardness profiles of each joint were consistent. The characteristic "W" hardness profile was exhibited by each joint. It is considered that the fine-grained microstructure in the SZ, by the effect of the dynamic recrystallization process, contributed to an increase in hardness.

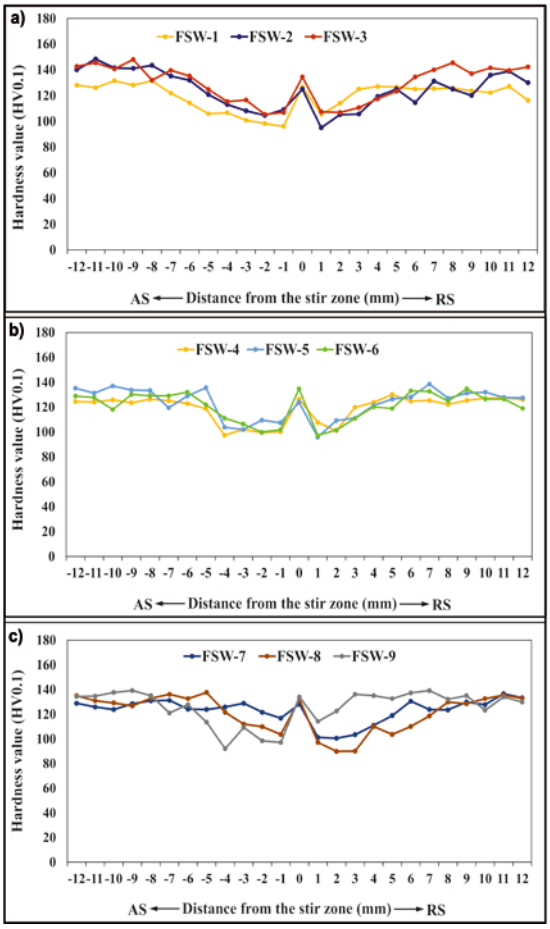


Fig. 11. Microhardness variation of welded joints.

The hardness values obtained in the center of the SZ region are close to the hardness value of the base metal. An increase in hardness value starting from the TMAZ towards to base metal has been observed. The second phase particles could be dissolved by the high-temperature action in SZ. The hardness of BM was measured to be higher than that of the SZ. The high hardness in BM might be due to the presence of second-phase particles. Changes in grain size from SZ to BM and a possible proportional decrease in second phase particles are considered influential in forming such a profile. On the basis of the SZ of the welded joints in Fig. 11a, the hardness values of FSW-3 on the AS were measured to be higher. FSW-1,2 and 3 welded joints demonstrated a hardness profile almost identical from the SZ to the BM on the AS (Fig. 11a). The change in hardness for the RS up to the TMAZ is similar to that of the AS, but there are significant differences in HAZ.

When comparing to the RS, FSW-1 shows lower values on the AS. FSW-4, 5, and 6 welded joints were produced at 630 rpm TRS. The change in hardness of the samples with the changing WS is shown in Fig. 11b. Considering the AS and RS, each welded joint's hardness profile was observed to be asymmetrical. The highest hardness values of FSW-4, 5, and 6 were 126 HV, 124 HV, and 135 HV, respectively. FSW-7, 8, and 9 welded joints were produced with the TRS of 800 rpm. The hardness of the welded joints with the changing WS is shown in Fig. 11c. The hardness profile of welded joints FSW-7 and FSW-8 exhibited a partially similar trend, having the highest hardness values in the SZ with a value of 128 HV and 132 HV, respectively. The highest hardness value in the SZ of the FSW-9 welded joint was measured to be 134 HV.

## CONCLUSIONS

The friction stir weldability of AA 7075-T651 aluminum alloy was investigated using three different TRS and WS. The welding combinations were utilized to investigate the influence of factors on the microstructural and mechanical attributes of joints. The following findings have been reached:

1. Cavity and void-type defects were observed on the welded joints obtained under the welding conditions of 400 rpm TRS and 40 and 63 mm/min WS. Similar-type defects were also observed on the welded joints produced using 630 rpm TRS and 63 and 80 mm/min WS. Defect-free joints were produced under the process parameter of 800 rpm TRS.
2. All of the joints exhibited onion rings.
3. While keeping TRS at a constant value, it was revealed that the grain size decreased with the increase in WS.
4. Coarser grain size with a value of 3.75 µm was measured under the welding conditions of 630 rpm TRS and 40 mm/min WS; however, the finest grain size with a value of 2.37 µm was measured under the FSW condition of 800 rpm TRS and 80 mm/min WS.
5. The highest UTS value (346 MPa) was achieved when TRS was set at 800 rpm TRS and 80 mm/min WS. The defective joints exhibited lower UTS and $\varepsilon_R$. While the FSW 1, 2, 3, 5, and 6 joints were fractured in SZ, the FSW 7-8 were fractured outside the SZ between HAZ and base metal-AS. The fracture site of FSW 4 was between HAZ and the base metal-RS.
6. The highest UTS efficiency was calculated to be 65% for FSW-9 welded joint; however, FSW-4 welded joint was the most ductile.

## COMPETING FINANCIAL INTERESTS STATEMENT

The authors declare that there are no conflicts of interest.

## ACKNOWLEDGMENT

This work has been supported by Yozgat Bozok University Scientific Research Projects Coordination Unit under grant number 6601a-FBE/20-396. The authors would like to acknowledge this financial support. The authors acknowledge the technical assistance of the Science and Technology Application and Research Center at Yozgat Bozok University. Tensile tests were performed at the Yozgat Bozok University Mechanical Engineering Department Materials Testing Laboratory (MATEL), which was funded by the "TANAP Social and Environmental Investment Programs".

## REFERENCES

Albannai, A.I., "Review The Common Defects in Friction Stir Welding," *International Journal of Scientific & Technology Research*, Vol.9, pp.318-329 (2020).

Backar, A., Elhofy, M., & Nassef, G., "Optimization of Friction Stir Welding Parameters of Al A9 1050-O with respect to Weld Tensile Strength and Soundness," *International Journal of Advanced Science and Technology*, Vol.29, No. 4s, pp.1322-1338 (2020).

Dehghani, K., Ghorbani, R., & Soltanipoor, A. R., "Microstructural Evolution and Mechanical Properties during the Friction Stir Welding of 7075-O Aluminum Alloy," *International Journal of Advanced Manufacturing Technology*, Vol.77, No.9-12, pp.1671-1679 (2015).

Farzadi, A., "Correlation between Precipitate Microstructure and Mechanical Properties in AA7075-T6 Aluminum Alloy Friction Stir Welded Joints," *Materialwissenschaft Und Werkstofftechnik*, Vol.48, No.2, pp.151-162 (2017).

Gemme, F., Verreman, Y., Dubourg, L., & Wanjara, P., "Effect of Welding Parameters on Microstructure and Mechanical Properties of AA7075-T6 Friction Stir Welded Joints," *Fatigue & Fracture of Engineering Materials & Structures*, Vol.34, No.11, pp.877-886 (2011).

Hua, L., Hu, X., & Han, X. H., "Microstructure Evolution of Annealed 7075 Aluminum Alloy and Its Influence on Room-Temperature Plasticity," *Materials & Design*, Vol.196, Paper No.109192 (2020).

Kah, P., Rajan, R., Martikainen, J., & Suoranta, R., "Investigation of Weld Defects in Friction-Stir Welding and Fusion Welding of Aluminium Alloys," *International Journal of Mechanical and Materials Engineering*, Vol.10, No.1, Paper No.26 (2015).

Kasman, S., & Ozan, S., "Effects of Overlapping Formed via Pin-Offsetting on Friction Stir Weldability of AA7075-T651 Aluminum Alloy," *Journal of Mechanical Science and Technology*, Vol.33, No.2, pp.819-828 (2019).

Kasman, S., & Ozan, S., "An Experimental Approach for Friction Stir Welding: A Case Study For AA 2024 - T351," *Sigma Journal of Engineering and Natural Sciences-Sigma Muhendislik Ve Fen Bilimleri Dergisi*, Vol.38, No.4, pp.1999-2011 (2020a).

Kasman, S., & Ozan, S., "Investigations on Microstructural and Mechanical Properties of Friction Stir Welded AA 2024-T351," *Materials Testing*, Vol.62, No.8, 793-802 (2020b).

Kumar, K., Kailas, S. V., & Srivatsan, T. S., "The Role of Tool Design in Influencing the Mechanism for the Formation of Friction Stir Welds in Aluminum Alloy 7020," *Materials and Manufacturing Processes*, Vol.26, No.7, pp.915-921 (2011).

Lakshminarayanan, A. K., Balasubramanian, V., & Elangovan, K., "Effect of Welding Processes on Tensile Properties of AA6061 Aluminium Alloy Joints," *International Journal of Advanced Manufacturing Technology*, Vol.40, No.3-4, pp.286-296 (2009).

Ma, Z. Y., Feng, A. H., Chen, D. L., & Shen, J., "Recent Advances in Friction Stir Welding/Processing of Aluminum Alloys: Microstructural Evolution and Mechanical Properties," *Critical Reviews in Solid State and Materials Sciences*, Vol.43, No.4, pp.269-333 (2018).

Mahoney, M. W., Rhodes, C. G., Flintoff, J. G., Spurling, R. A., & Bingel, W. H., "Properties of Friction-Stir-Welded 7075 T651 Aluminum," *Metallurgical and Materials Transactions a-Physical Metallurgy and Materials Science*, Vol.29, No.7, pp.1955-1964 (1998).

Mao, Y. Q., Ke, L. M., Chen, Y. H., Liu, F. C., & Xing, L., "Improving Local and Global Mechanical Properties of Friction Stir Welded Thick AA7075-T6 Joints by Optimizing Pin-Tip Profile," *International Journal of Advanced Manufacturing Technology*, Vol.88, No.5-8, pp.1863-1875 (2017).

Mao, Y. Q., Ke, L. M., Liu, F. C., Huang, C. P., Chen, Y. H., & Liu, Q., "Effect of Welding Parameters on Microstructure and Mechanical Properties of Friction Stir Welded Joints of 2060 Aluminum Lithium Alloy," *International Journal of Advanced Manufacturing Technology*, Vol.81, No.5-8, pp.1419-1431 (2015).

Ozan, S., "Effect of Friction Stir Welding on the Microstructure and Mechanical Properties of AA 6063-T6 Aluminum Alloy," *Materialwissenschaft Und Werkstofftechnik*, Vol.51, No.8, pp.1100-1119 (2020).

Ozan, S., Sahin, S., & Kasman, S., "Effects of parameters on friction stir welding process of AA 7075 aluminum alloy: mechanical and microstructural assessments," Materialwissenschaft Und Werkstofftechnik, Vol.53, No.9, pp.1128-1143 (2022).

Patel, V. V., Badheka, V., & Kumar, A., "Effect of Polygonal Pin Profiles on Friction Stir Processed Superplasticity of AA7075 Alloy," *Journal of Materials Processing Technology*, Vol.240, pp.68-76 (2017).

Rajak, D. K., Pagar, D. D., Menezes, P. L., & Eyvazian, A., "Friction-Based Welding Processes: Friction Welding and Friction Stir Welding," *Journal of Adhesion Science and Technology*, Vol.34, No.24, pp.2613-2637 (2020).

Rajakumar, S., Muralidharan, C., & Balasubramanian, V., "Influence of Friction Stir Welding Process and Tool Parameters on Strength Properties of AA7075-T-6 Aluminium Alloy Joints," *Materials & Design*, Vol.32, No.2, pp.535-549 (2011).

Rezaei, H., Mirbeik, M. H., & Bisadi, H., "Effect of Rotational Speeds on Microstructure and Mechanical Properties of Friction Stir-Welded 7075-T6 Aluminium Alloy," *Proceedings of the Institution of Mechanical Engineers Part C-Journal of Mechanical Engineering Science*, Vol.225, No.C8, pp.1761-1773 (2011).

Sadoun, A. M., Meselhy, A. F., & Deabs, A. W., "Improved Strength and Ductility of Friction Stir Tailor-Welded Blanks of Base Metal AA2024 Reinforced with Interlayer Strip of AA7075," *Results in Physics*, Vol.16, Paper No.102911 (2020).

Seidel, T. U., & Reynolds, A. P., "Visualization of the Material Flow in AA2195 Friction-Stir Welds Using a Marker Insert Technique," *Metallurgical and Materials Transactions a-Physical Metallurgy and Materials Science*, Vol.32, No.11, pp.2879-2884 (2001).

Shah, P. H., & Badheka, V. J., "An Experimental Insight on the Selection of the Tool Tilt Angle for Friction Stir Welding of 7075 T651 Aluminum Alloys," Vol.9, No.S1, pp.1-11 (2016).

Sharma, C., Dwivedi, D. K., & Kumar, P., "Effect of Welding Parameters on Microstructure and Mechanical Properties of Friction Stir Welded Joints of AA7039 Aluminum Alloy," *Materials & Design*, Vol.36, pp.379-390 (2012).

Sharma, C., Dwivedi, D. K., & Kumar, P., "Fatigue Behavior of Friction Stir Weld Joints of Al-Zn-Mg Alloy AA7039 Developed Using Base Metal in Different Temper Condition," *Materials & Design*, Vol.64, pp.334-344 (2014).

Thomas, W. M., "Friction Stir Welding and Related Friction Process Characteristics," Proc. 7th International Conference Joints in Aluminium (INALCO'98), Cambridge, (1998).

Thomas, W. M., Johnson, K. I., & Wiesner, C. S., "Friction Stir Welding-Recent Developments in Tool and Process Technologies," *Advanced Engineering Materials*, Vol.5, No.7, pp.485-490 (2003).

Utyaganova, V., Filippov, A., Tarasov, S., Shamarin, N., Gurianov, D., Vorontsov, A., . . . Kolubaev, E., "Characterization of AA7075/AA5356 Gradient Transition Zone in an Electron Beam Wire-Feed Additive Manufactured Sample," *Materials Characterization*, Vol.172, Paper No.110867 (2021).

Xu, W. F., Li, Z. X., & Sun, X. H., "Effect of Welding Speed on Mechanical Properties and the Strain-Hardening Behavior of Friction Stir Welded 7075 Aluminum Alloy Joints," *Journal of Materials Engineering and Performance*, Vol.*26*, No.4, pp.1938-1946 (2017).

Zhang, Y. N., Cao, X., Larose, S., & Wanjara, P., "Review of Tools for Friction Stir Welding and Processing,". *Canadian Metallurgical Quarterly*, Vol.51, No.3, pp.250-261 (2012).

Zou, X. L., Yan, H., & Chen, X. H., "Evolution of Second Phases and Mechanical Properties of 7075 Al Alloy Processed by Solution Heat Treatment," *Transactions of Nonferrous Metals Society of China*, Vol.27, No.10, pp.2146-2155 (2017).